Line Narrowing of Fiber Coupled Laser Diode Array
and ^{3}He Lung MRI

by

Jermane E. Massey

B.A., Physics (1994)

Hampton University

Submitted to the Department of Physics in Partial
Fulfillment of the Requirements for the Degree of
Master of Science in Physics

at the

Massachusetts Institute of Technology

September 1999

Signature of Author. . . . .
Department of Physics
September 3, 1999

Certified by . . . .
Ron Walsworth
Harvard-Smithsonian Center for Astrophysics
Thesis Supervisor

Accepted by. . . . .
Thomas J. Greytak
Associate Professor, Department Head for Education

Line Narrowing of Fiber Coupled Laser Diode Array and ^{3}He Lung MRI

by

Jermane E. Massey

Submitted to the Department of Physics in Partial
Fulfillment of the Requirements for the Degree of
Master of Science in Physics

ABSTRACT

An experimental study was performed to determine the gains achievable through injection locking of a laser diode array (LDA) as a means to improve optical pumping rates of Rb for spin exchange polarization of ^{3}He. For fiber coupled laser diode arrays, gains (~ 2) were limited by light polarization, coupling efficiency, and incidence angle. With the bare LDA (operated at $1.5I_{threshold}$) average gains of 35 were seen with < 2mW of injected power.

A novel MRI coil and polarization system were developed for hyper-polarized ^{3}He lung imaging at 3 T. Initial ^{3}He nuclear spin polarization of ~ 2% was achieved.

Thesis Supervisor: Ronald L. Walsworth

Injection Locking of High Power Laser Diode Arrays

Diode lasers have become a common tool for atomic physics experiments, laser spectroscopy, and polarizing noble gases. Thus more attention has been given to improving their performance. Some of their limitations stem from frequency stability, spatial beam quality, spectral width, and low power output.[1] Recently, near infrared laser diode arrays (LDAs) have been produced with very high output powers (tens of watts) but also, large spectral widths (1–3 nm). For our optical pumping application -spin-polarizing an atm-liter or so of ^{3}He or ^{129}Xe gas- only a small fraction of the LDA power was resonant with the Rb transition. To maximize the rate of noble gas spin polarization we were interested in increasing the LDA power at the Rb D1 transition (wavelength ≈ 794.7 nm, linewidth pressure broadened by the noble gas to ~10-50 GHz).

Several techniques exist for enhancing the narrow band resonant power of semiconductor diode lasers, including optical feed back[2,3] and injection locking[1,4,5,6]. In injection locking, a narrow band, low power "master laser" (ML) emits light at a single mode. This low power beam is injected into the broadband high power "slave laser" (SL), thus forcing the SL to oscillate in response to the driving ML. Here we have studied injection locking of Opto Power multi-stripe LDAs which emit 15 watts of total power. Both optical fiber

coupled and uncoupled LDAs were investigated. Fiber coupled LDAs have practical advantaged: circularizing the output light's beam profile; and efficient transport of light from LDA to optical pumping cell.

Fiber Coupled LDA

In our injection locking studies we used a Ti:Sapphire laser as the "master laser". This high power narrow band laser (Spectra Physics model number 3900S) is pumped by an Argon-ion laser (Spectra Physics model number 2040E) and has a linewidth much narrower than the pressure broadened Rb line. The 6 watts of maximum Ti:sapphire output power greatly exceed the amount needed for these tests. Therefore the ML was typically run close to threshold, emitting tens to hundreds of milliwatts, as needed. The "slave laser" (Opto Power model number OPC-A015-FCPS) consisted of 24 integrated 20 stripe diode arrays and had a total output power of 15 watts. The light output from the front facet of each array was coupled via a microlens into a multi-mode optical fiber (cladding diameter = 275 μm, core diameter = 250 μm). The 24 fibers were bundled in a metallic sheath that terminated in an SMA connector. The rear facet of each array was sealed inside the laser package. Because of the one-to-one

correspondence between the 24 individual diode arrays and

fibers, we refer to each fiber-array pair as a "single

fiber," and the complete fiber-array set as the "full fiber

bundle." Each of the twenty-four fibers emitted up to 600 mW

of 795 nm light for a total of 15 watts.
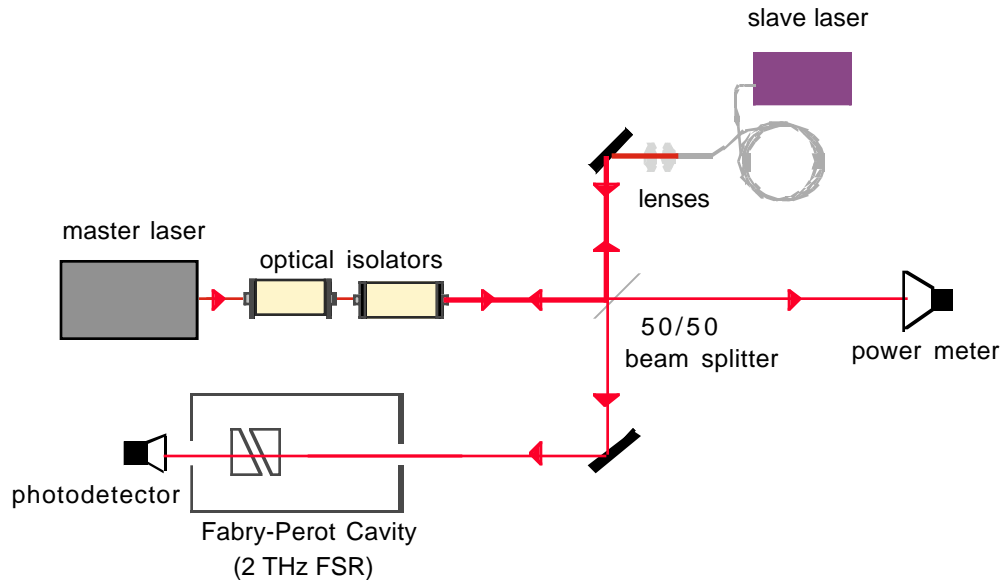
Figure 2. Experimental setup used in injection locking studies of fiber-
coupled LDAs. The master laser (ML) light passes through a pair of
optical isolators before a 50/50 beamsplitter sends half of the light
into the slave laser (SL). The remaining light travels directly into a
power meter allowing on-line monitoring of ML power. The output of the
SL is directed into a Fabry Perot spectrum analyzer.

Previous studies[1-5] coupled the injected light directly

onto the face of the diode lasers. Ours was the first attempt

to injection lock a multi-mode fiber coupled array. The

multimode fiber scrambles the polarization of the injected

light, reducing the light in any single mode that is

available for injection locking of the broadband high power

slave laser (SL). The commercially installed fiber also

prevents us from varying the angle of incidence of the
injected light onto the LDA.
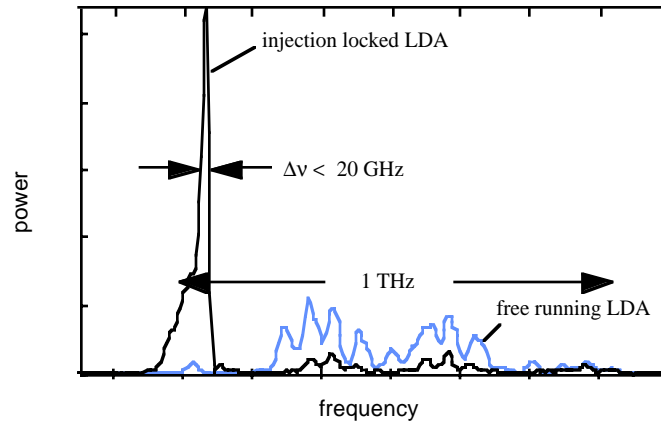
Figure 3. Single fiber spectral outputs. The free running SL output is
shown in gray, with a width of nearly 1 THz. The injection locked
output (superimposed) shows nearly all of the SL power within a line
less than 20 GHz wide. [7]

    The gain realized by injection locking the free running
LDA was the ratio of SL power in the injection locked peak to
the total power of the ML injected light. In practice, the
gain was calculated by measuring the narrow line fraction,

$$f = \frac{P_{IL}}{P_{LDA}}.$$

where P_{IL} is the power in the injection locked peak and P_{LDA} is
the total output LDA power as measured with a Fabry-Perot
spectrum analyzer (see Figure 2). In calculating P_{IL}, the ML
light reflected off the SL was subtracted from the injection
locked spectrum. After measuring the total powers of the LDA
and the ML (Ti:sapphire), the gain is given by,

$$G = \frac{P_{IL}}{P_{Ti}}.$$

Figure 3 shows our typical observed injection locking of a single fiber, where we were able to collapse 72% of the 1 THz LDA output into a FWHM linewidth of <20 GHz. However, the observed gain, G, was only ~4, which is not a great enhancement. Our measurements indicated that this inefficiency was due to a number of master laser power loss mechanisms. Light was being reflected off the fiber surfaces and the polarization was randomized as it traversed the fiber. Furthermore, the fiber prevented controlling the focus of the injected ML light onto the SL. Despite these factors, we used injection locking to achieve significant spectral narrowing of a ~ 625 mW fiber-coupled Opto Power LDA. Thus we conclude that injection locking of fiber-coupled LDAs –at least as currently manufactured- is not a practical technique for improved spin exchange optical pumping of noble gases.

Uncoupled LDA

To confirm the hypothesis that power loss was limiting the injection locking gain in fiber-coupled LDAs, we investigated an Opto Power LDA with no fiber coupling. This

allowed us to control the polarization, incident angle, and spot size of the injected ML (Ti:Sapphire) light.
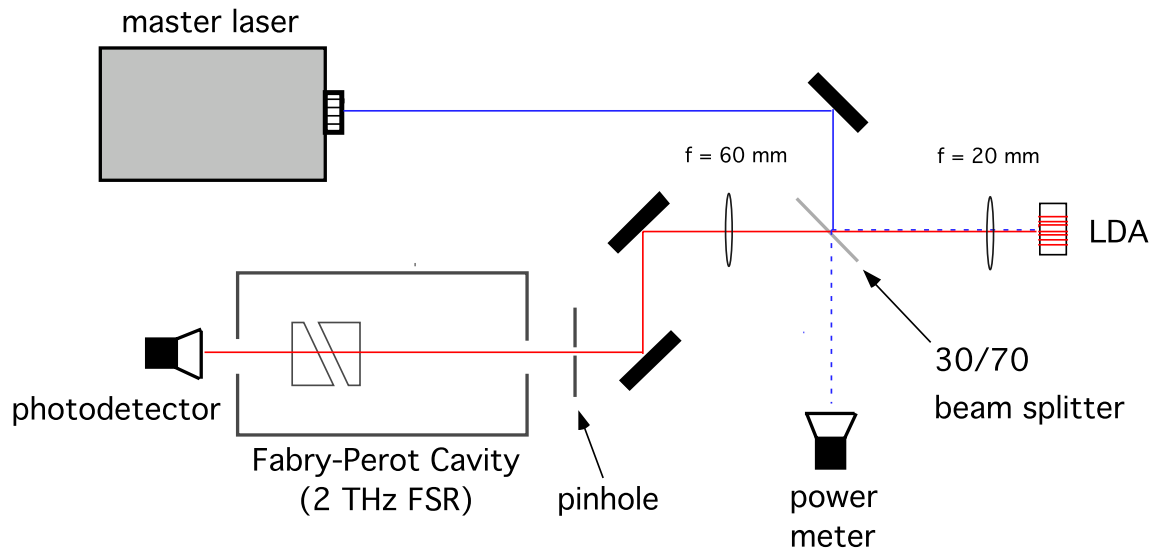
Figure 4. Experimental setup for injection locking studies of an uncoupled Opto Power laser diode array.

Experimental Setup and Results

Again we used the Ti:Sapphire as the ML. The SL was an uncoupled (no fiber) Opto Power LDA. The experimental set-up is shown in Figure 4. The optical isolators were removed because the large divergence (> 30˚)of the uncoupled LDA allowed us to neglect any coupling effects between the ML and SL (e.g., reflection of ML light into Fabry-Perot spectrum analyzer). The LDA consisted of 24 individual laser diode arrays spaced 200 μm apart, the same as the fiber coupled array. Each array was made up of 20, 3.5 μm wide, diode stripes, separated by 6.5 μm.[8] A beamsplitter and spherical lens that focused the ML light onto the SL were affixed to a

X-Y translation stage. The SL was monitored using a Fabry-Perot optical spectral analyzer (Burleigh Instruments, RC-140) with a free spectral range of approximately 2 THz and a finesse of 100. A 20 mm focal length lens was used to focus the Ti:Sapphire light onto one of the 24 diode arrays. With the 20 mm lens we were able to focus down to a diameter of 28 μm (at 1/e intensity points). Given the dimensions of a single array, (200 μm x ~0.1 μm)[9] a large percentage of the injected light fell outside of the active region of the LDA, necessarily reducing the net gain of the injection locking technique (results given below).

Nonetheless, with the bare LDA we were able to achieve more efficient injection locking than with fiber-coupled LDAs. In Figure 5 the measured injection locking gain is plotted vs. ML power, showing an average gain of about 35 using ~ 1 mW of injected ML power. However, this larger gain occurs with a small narrow line fraction (f ~ .30). To achieve a practically useful narrow line fraction (f ~ 0.70), larger ML powers must be used (~ 80 mW for a single diode array), which reduces the injection locking gain to ~ 2.
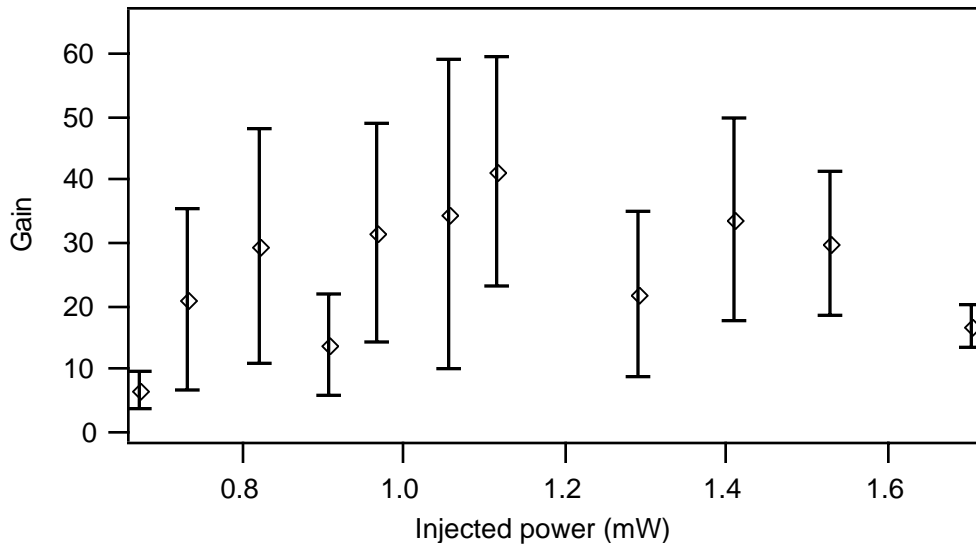
Figure 5. Injection locking gain as a function of ML power for a single uncoupled diode array. The average gain was calculated from ten consecutive measurements taken 3 seconds apart. The error bars represent the standard deviation.
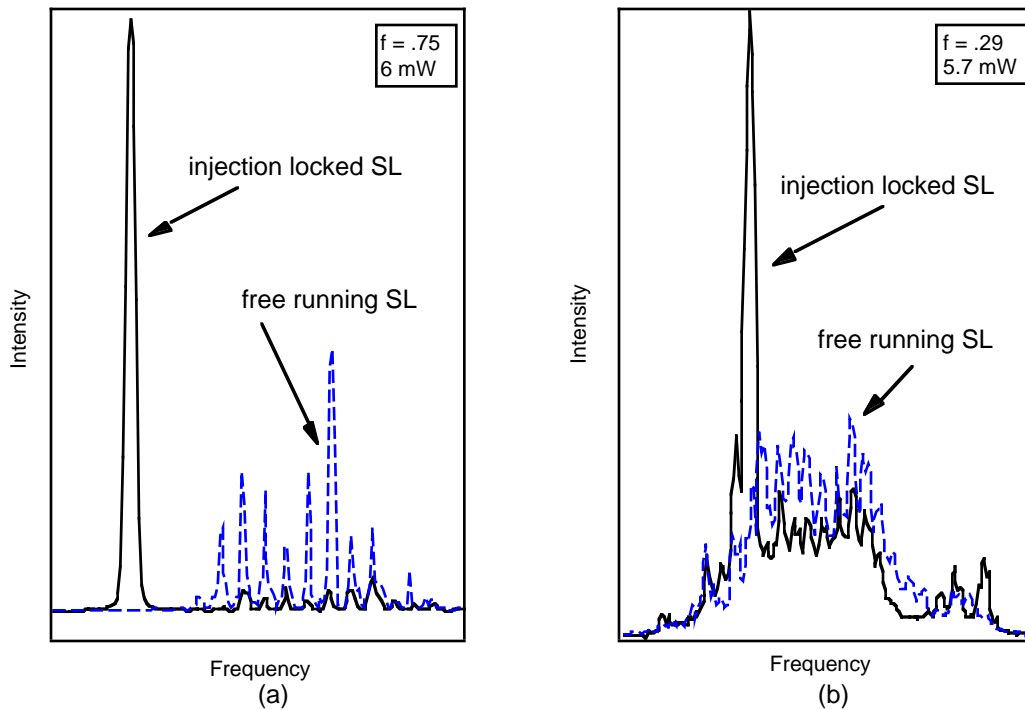
Figure 6. (a) Off resonant injection locking spectrum for a single, uncoupled diode array. (b) Near resonant injection locking spectrum at an off axis angle of 2 degrees.

Other researchers have found that injection locking gain can be improved when the ML light is incident on the LDA facet at small angles from normal[4,13]. We found maximum gains with an incident angle of about 2 degrees, with the gains increased by ~ 10% compared to normal incidence. For example, Figure 6b, shows the injection locked SL spectrum for 5.7 mW of ML light injected into the SL running at 26.2A, which corresponds to a total SL power output of ~ 600 mW for each of the 24 diode arrays in the LDA. Here, the narrow line fraction, f, was 0.29, and the gain was 30.5. Beyond this 2˚ incident angle both the measured narrow line fraction and gain fell off. At angles > 5˚ no injection locking was observed.

In addition to ML power and incident angle we investigated the effect of changing ML polarization. To do so, a quarter wavelength plate was placed between the ML and SL, to circularly polarize the injected light (i.e., to make the injected light a superposition of horizontally and vertically polarized light). With the circularly polarized injected light, a 50% decrease in the injection-locking efficiency was observed, which implied that only the horizontally polarized ML light was contributing to the injection locking. This confirmed that the destruction of ML polarization by the optical fiber was a large factor in the poor injection locking of the fiber-coupled LDA. The multi-

mode fiber randomized the polarization, so only 50% of the

light transmitted through the fiber had the proper

polarization for injection locking.

(a) no voltage

p-type semiconductor | Junction | n-type semiconductor

conduction band

holes

valence band

(b) voltage applied, current flows, light emitted

recombination of holes and electrons
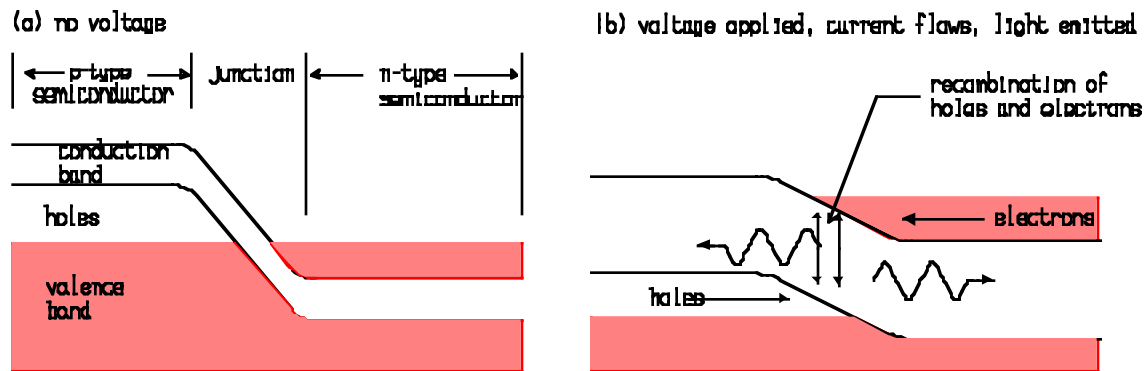
electrons

holes

Figure 7. Schematic of p-n junction used in diode lasers. When current flows across the junction, holes and electrons recombine; i.e., electrons relax from the conduction band to the valence band. The relaxation energy is released as photons.

We also found that the injection locked SL peak was

slightly shifted ~20 GHz, from the injected ML frequency.

Standard diode laser physics provides a clear explanation for

this shifting. When a p-type semiconductor is joined with a

n-type semiconductor a conduction band gap is formed (see

Figure 7). Forward biased voltage applied across this p-n

junction, stimulates the relaxation of the holes and

electrons, which thereby emit radiation. If the population of

holes and electrons is made large enough through doping and

the voltage is large enough, a population inversion can be

induced in the junction area.[10] With the proper index of

refraction at the ends of the junction, to sustain repeated amplification, laser action can be achieved.

The observed shift between the ML and SL frequency is caused by a change of the index of refraction due to carrier depletion in the SL's junction region (see Figure 7). When light is injected, the output of the SL slightly increases; i.e., more photons are emitted. Since photons are only emitted after holes recombine with electrons, the result is a decrease in the carrier density in the junction region of the laser diode. This decrease in the carrier density increases the refractive index, which lowers the SL cavity resonance frequency. Therefore, the injection locked SL output frequency was slightly downshifted from the ML frequency[11].

Future work

Coupling of the injected light to the LDA was limited by the spot size. With improved optics more of the ML light would be injected into the active region of the LDA, thereby improving the gain. The coupling efficiency could also be improved by using anti-reflective coated lenses. Also practical use of injection locking to improve spin exchange optical pumping of noble gases will require the injection-locked SL output to be more stable. The SL spectra we recorded were rapidly acquired scans of a fluctuating signal

that varied in power by factors of ~ 2 over seconds. We believe this effect was caused by intensity beats, a result of the interaction of the locked and unlocked SL modes.[12] Another factor that contributed to injection locking instability was manual temperature control of the LDA. An improved temperature control system providing 0.1 K stability is needed to keep the LDA injection locked for lengthy periods (~ hours). Finally, we note that a practical LDA injection locking system would require a small, inexpensive, and robust master laser (not a Ti:sapphire/argon-ion laser).

Conclusion

We demonstrated injection locking of high power, near infra-red laser diode arrays (LDA), both with and without multi-mode optical fibers coupling the LDA light. For the fiber coupled LDA, this technique narrowed more than 72% of the output LDA light into a spectral width of less than 20 GHz. Unfortunately, scrambling of the injected light polarization, reflections, and lack of control of the injected light focus and angle, make it likely that injection locked gains at 10 or greater cannot be achieved with a fiber coupled LDA.

[1] S. Shang and H. Metcalf, Appl. Opt. **28**, 1618 (1989).
[2] K. Peterman and G. Arnold, J. Quant. Elect. **QE-18**, (1982).
[3] W.J. Burke et al., Appl. Opt. **17**, 2233 (1978).

[4] L. Goldberg et al., Appl. Phys. Lett. **46**, 236 (1985).

[5] H. Tsuchida, Opt. Lett. **19**, 1741 (1994).

[6] R. Lang, IEEE J. Quantum Electronics **QE-18**, 976 (1989).

[7] M. Humphrey, unpublished.

[8] Private communication with Opto Power

[9] Opto Power specifications.

[10] D. O'Shea, "An Introduction to Lasers and their Application." (1997)

[11] R. Lang, IEEE J. Quantum Electronics **QE-18**, 976 (1989).

[12] K. Otsuka and S. Tarucha, IEEE J. Quant. Elect. **QE-17** 1515 (1981).

Development of Hyper-polarized [3]He Gas Imaging of the Lung at 3T

Spin exchange optical pumping greatly enhances the detectable NMR signal of [3]He gas. Our aim was to develop new image selectivity and contrast techniques for hyper-polarized [3]He MRI of the human lung at a magnetic field strength of 3 tesla, twice the field strength of most clinical full body MRI systems. This increased field strength offers unique opportunities for improved image quality, better spectral resolution, and enhanced image contrast due to larger magnetic susceptibility effects.[1] For this work we used a state-of-the-art 3T MRI system located at the Massachusetts General Hospital (MGH): a GE-ANMR 3T 80cm bore whole body instrument (see photograph in Figure 8). To perform human lung [3]He MRI at 3T we also had to develop special whole-body RF coils, a heterodyne system to detect [3]He NMR signals, and construct a system to provide ~1 liter of hyper-polarized [3]He gas for human inhalation.

Figure 8. Photograph of the GE-ANMR 3 T full body system with subject positioned in volume chest coil

Basic Principles of NMR

NMR stems from the interaction of the magnetic moment of a nucleus with a magnetic field. The first NMR signals were detected by Felix Bloch, and independently Edward Purcell in 1946.[2] Nuclei possess intrinsic spin and an associated magnetic moment[3]

$$\mu = \gamma \mathbf{S},$$

where γ is the gyromagnetic ratio of the nucleus. The gyromagnetic ratios of interest are those for ^{1}H and [3]He:

$$\gamma_{^3He} = 20.38\,krad/s \cdot gauss = 32.44\,MHz/T$$
$$\gamma_{^1H} = 26.73\,krad/s \cdot gauss = 42.58\,MHz/T$$
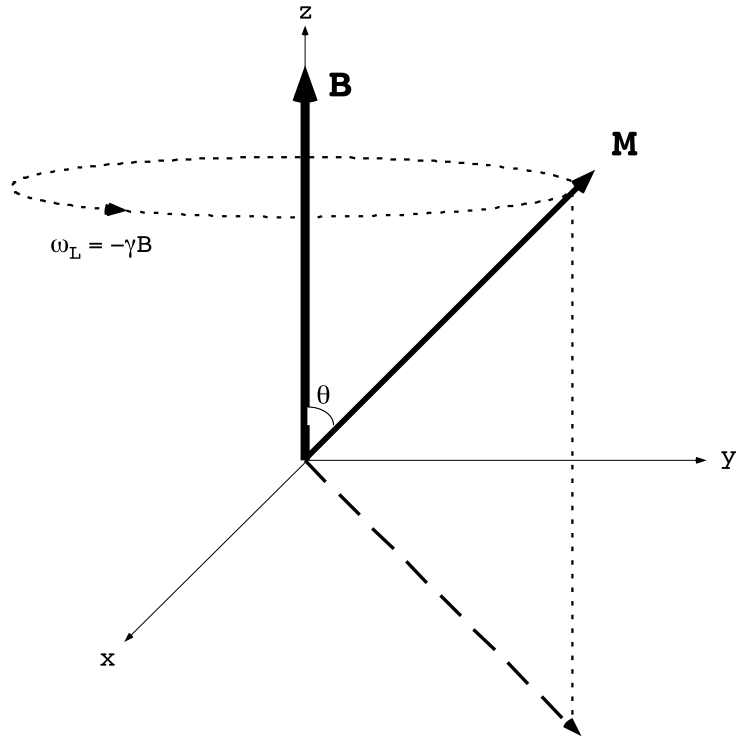
Figure 9. Precession of the magnetization about a constant B field after being tipped by angle θ.

The intrinsic spin, **S**, of the nucleus interacts with the magnetic field, **B**, such that there are only an integer number of energy states. While this effect is completely described using quantum mechanics, for this discussion a classical explanation will suffice.

Classically **S** can be considered equivalent to L, the angular momentum. When magnetic moments are placed in a uniform magnetic field $\mathbf{B} = B\hat{z}$, they experience a torque,

$$\mathbf{N} = \mu \times \mathbf{B} = \frac{d\mathbf{S}}{dt}.$$

This torque causes the magnetic moment (or magnetization, $\bar{M}$, for an ensemble of nuclear spins) to precess about the

direction of the field (see Figure 9). By solving the equation of the time derivative of the spin angular momentum,

$$\frac{d\mathbf{S}}{dt} = \mathbf{S} \times \gamma\mathbf{B} = -SB\gamma \sin\theta\hat{\Phi},$$

we get the spin precession or Larmor frequency,

$$\omega_L = -\gamma B.$$

Isotopes with nuclear spin = 1/2 are most often used in NMR, because they have are abundant and do not have higher order electromagnetic moments which shorten the spin polarization and coherence lifetimes by enhanced coupling to the environment. The energy of a nucleus with spin in the presence of a magnetic field has two distinct energy levels,[4,5]

$$E = \pm\frac{1}{2}\hbar\omega_L.$$

These two energies correspond to the magnetic moment anti-parallel and parallel to the magnetic field, $\mathbf{B}$. This energy splitting due to the field $\mathbf{B}$ is the nuclear Zeeman effect. The difference in the number of nuclei in parallel and anti-parallel states results in a net magnetization. For a sample in thermal equilibrium the excess of uncanceled spins aligned parallel with the $\mathbf{B}$ field can be calculated using the Maxwell-Boltzmann distribution.

$$N_\pm = N_o e^{\mp\frac{\mu B}{k_B T}},$$

where $k_B = 1.380 \times 10^{-23} \dfrac{J}{K}$, and $\pm$ is used to represent a nucleus with its magnetic moment parallel ($-$) or anti-parallel ($+$) to the applied field. And the net magnetization is given by

$$M = N_o \mu \frac{N_+ - N_-}{N_+ + N_-}$$

$$= N_o \mu \tanh\left(\frac{\mu B}{k_B T}\right)$$

$$= N_o \mu \tanh\left(\frac{\hbar \omega_L}{2 k_B T}\right)$$

$$\approx N_o \mu \left(\frac{\hbar \omega_L}{2 k_B T}\right), \quad \text{for } \hbar \omega_L \ll 2 k_B T.$$

At room temperature for ^{3}He in a 3T field the Boltzmann factor is 7.74×10^{-6}.

Transverse RF magnetic fields, resonant with the Zeeman transition (i.e., at the Larmor frequency), are used to tip the magnetization away from the z axis. In the rotating frame of the magnetic moment, the resonant RF field is fixed. If this RF excitation pulse is applied for time t_p, the tip or flip angle (i.e., the angle by which the magnetization is rotated away from the z-axis) is

$$\theta = \arcsin\left(\gamma B_1 t_p\right) \approx \gamma B_1 t_p \qquad \text{for small tip angles,}$$

where B_1 is the magnitude of the applied transverse RF field. Following this pulse a portion of the magnetization is now in the transverse plane rotating about the z axis (see Figure 10).
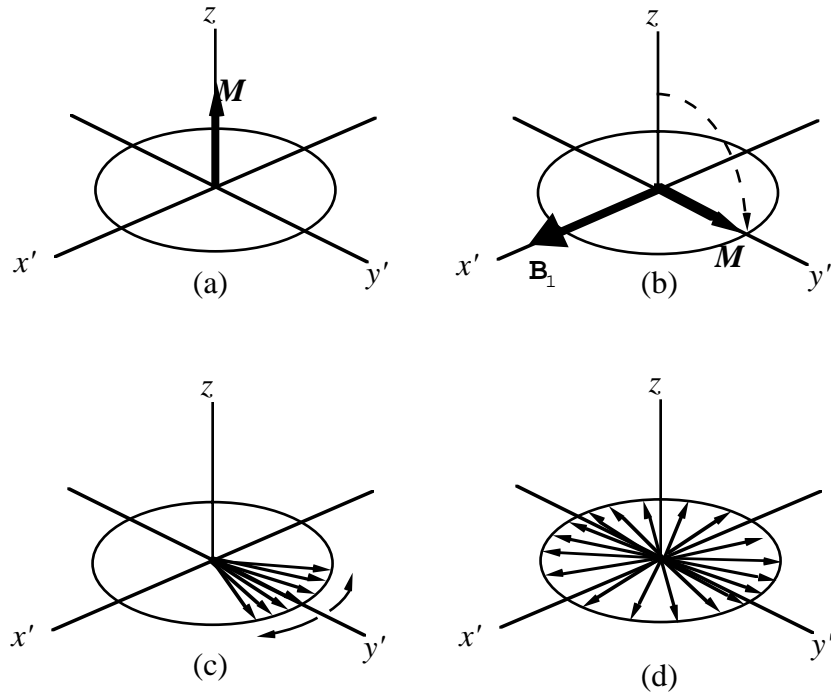
Figure 10. (a) Magnetization lies along the z-axis, initially (the static magnetic field along the z-axis is not shown). (b) A transverse resonant magnetic field tips the magnetization into the x'-y' plane (i.e., the transverse reference frame rotating at the Larmor frequency relative to the fixed lab frame, x-y). (c) Individual spins begin to dephase due to atomic interactions, etc. (d) Spins are completely dephased.

By Faraday's law, this magnetization rotating at the Larmor frequency can induce a current in a nearby pickup coil. With the coil tuned to the resonant frequency and the proper electronics this NMR signal can be sensitively detected.

The precession of the transverse magnetization does not continue indefinitely. Interactions with neighboring atoms and magnetic field inhomogeneities cause the nuclear spin ensemble to lose phase coherence, and the NMR signal to decay -typically exponentially with some characteristic time. This decaying NMR signal, $S(t)$, is called the free induction decay

(FID), and the characteristic time is labeled T_2^*. If the B_1 tipping pulse occurs at t=0, then

$$S(t) = S_o \sin(\theta)\cos(\omega_L t)e^{-\frac{t}{T_2^*}}.$$

Thus the largest detectable signal is produced with a 90˚ flip angle.

In 1973, Mansfield and Grannell[6] demonstrated the relationship between NMR signals and spatial variations in spin density using Fourier techniques. To form an image, spatial encoding of the magnetization density is needed. In Magnetic Resonance Imaging (MRI) magnetic field gradients are applied to encode position information. Spins experiencing different fields rotate at different frequencies. When a strong gradient is applied, the sampling volume is divided into slices along the z axis with different **B** fields (see Figure 11). This slice selection, in combination with x-y axis frequency and phase encoding magnetic field gradients, creates a map of NMR signal strength in frequency-space (known as k-space). When Fourier transformed, this information can be used produce a tomographic image of spin density or other NMR observables in position space.
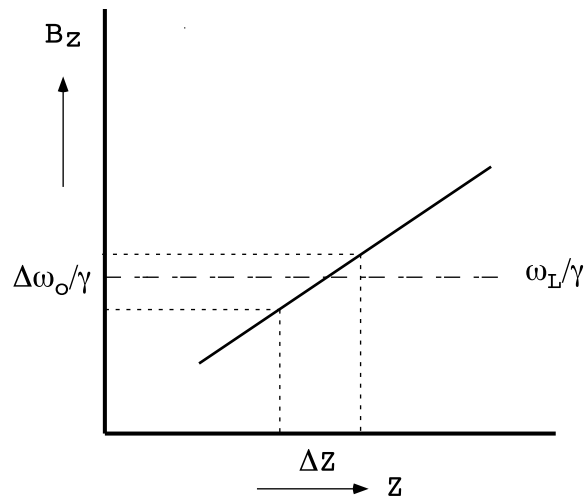
Figure 11. The z-gradient field is a function of position. Along the z axis the field increases linearly. A detection bandwidth $\Delta\omega$ around the Larmor frequency determines a slice ΔZ along the z axis from which NMR signals are detected.

[1] R.L. Walsworth, NASA research proposal.

[2] K.H. Hausser and H.R. Kalbitzer, "NMR in Medicine and Biology" (Springer-Verlag, New York,1988) p. 1.

[3] R. Shankar, "Principles of Quantum Mechanics",(Plenum Press, New York, 1980).

[4] E. Purcell, "Electricity and Magnetism", (McGraw-Hill, 1985) pp. 414 - 420.

[5] R.L. Walsworth, NASA research proposal.

[6] P. Mansfield and P.K. Grannell, J. Phys. **C6**, L422 (1973).

Development of Signal Detection Electronics for ^{3}He NMR at 3T

We developed the technology for human lung MRI of hyper-polarized ^{3}He gas at a field twice that of current routine clinical fields (3 tesla). Working at 3 T offers unique challenges and benefits. The higher field creates better ^{3}He image contrast to highlight lung tissue structure and changes, while the larger Larmor frequency makes it more difficult to maintain B_1 homogeneity across the human chest. For the most efficient stimulation and detection of the NMR signal, the B_1 field should be aligned normal to the **B** field. In clinical imaging systems the static **B** field is usually aligned with the long axis of the patient (head to toe), eliminating the use of the simple but effective solenoid coil for creating and detecting B_1. In addition, at high frequencies the physical length of single or double loop surface coils are longer than $\frac{\lambda}{4}$, resulting in spatial inhomogeneity in the B_1 field.

For our investigations, therefore, we developed a third type of coil, a whole-chest volume coil (see Figure 12). Unlike surface coils which have one loop laid flat to produce the orthogonal field, volume coils produce a field that is transverse to their cylindrical axis. A continuous sinusoidal current distribution around the circumference of the

cylinder, and a current flux along the axis are required to produce such a field[1].

Our whole-chest volume coil was an adaptation of a bird cage coil, driven in quadrature. A typical bird cage coil is made of lumped LC elements in a ladder network inductively coupled to two outer rings. Our coil eliminated the outer rings in favor of capacitive coupling to a larger cylindrical conductive tube encircling the axis elements, resulting in a transverse electromagnetic circuit with transmission line elements. This design yields maximum B_1 homogeneity within the cylinder.
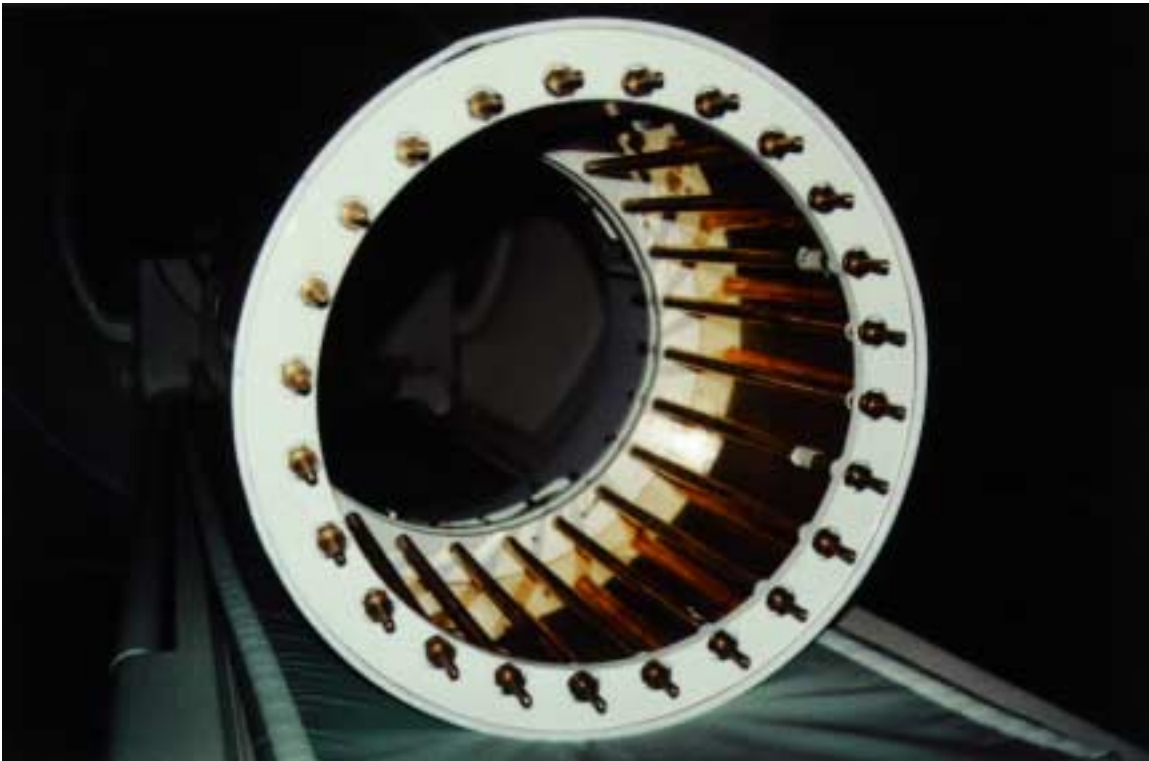
Figure 12. Photograph of the 24 element volume chest coil.

Precessing nuclei have two orthogonal oscillating magnetization components in the lab frame. A linearly polarized coil can only stimulate one of these components. Driving the coil in quadrature reduces the required RF power by a factor of two because it produces a circularly polarized B_1 field that precesses with the excited magnetization, stimulating both components.[2,3] Similarly, we operated the volume coil in quadrature to allow both orthogonal components of the rotating ^{3}He magnetization to be detected. The RMS noise voltage of the two components are incoherent, so the net S/N increases by a factor of $\sqrt{2}$.

As a test , we used the new chest coil to obtain axial thoracic ^{1}H images at 3 T of a human volunteer (see Figure 13). This image clearly shows blood vessels in the lung: but a signal void in the lung gas space -a void to be filled with ^{3}He images in future work.

Figure 13. Axial ^{1}H images at 3 T of a 1 cm thick cross-section of the thorax of a human volunteer, obtained with new whole-chest coil. Note the signal void in the lung gas space. Hyper-polarized ^{3}He MRI will provide complimentary, high-resolution gas space images of the lung.

Processing of the ^{3}He NMR signal required us to build a heterodyne front end to bypass the GE receiver and transmitter electronics. Most NMR imaging systems are designed to detect ^{1}H spins in water and other tissues, which have a resonant frequency of 127.72 MHz at 3 T, whereas our whole-chest volume coil was tuned to 97.30 MHz, the Larmor frequency of ^{3}He. To use the coil on the 3T system the RF signals received and transmitted had to be mixed up to 127.72 MHz on the receiver end and mixed down to 97.30 MHz on the transmit side. A schematic of the changes made to the GE electronics is given in Figure 14.

Figure 14. Schematic of 3 T multinuclear RF front end.

Development of a ^{3}He Hyper-Polarization System

Spin exchange collisions with optically pumped[4] alkali metal atoms can polarize noble gas atoms nuclear spins (e.g., ^{3}He). In our hyper-polarization system we optically pump Rb to transfer polarization to the ^{3}He atoms. Rubidium is convenient because its D1 transition is in the near infra-red, falling within the range of available high-power laser diode arrays (LDAs), and Rb has a high vapor pressure at reasonable temperatures. Pressure broadening due to ^{3}He and N_2 gas increases the optical pumping rate by allowing more of the LDA light to interact with the Rb. The D1 transition of Rb is excited using circularly polarized light at 795.

As can be seen in Figure 1, only Rb atoms in the $m_s = -1/2$ state absorb the circularly polarized light, and make the transition to the excited state. The atoms could return to the ground state sublevels via spontaneous emission. However, the emitted photons can be reabsorbed by other Rb atoms. This effect known as radiation trapping, would reduce the Rb spin polarization, but was compensated for by including a buffer gas, N_2. Through collisions with the N_2, the excited Rb atoms are relaxed to the ground state without emitting radiation. This evenly distributes the Rb atoms into the ground state sublevels. Thus, over time the probability of finding Rb atoms in the $m_s = 1/2$ state increases relative to that of the

m_s = -1/2 state. This process is called depopulation optical pumping.

The photon absorption rate of the Rb vapor, γ_{opt}, is linearly dependent on the flux of incident σ^+ polarized light. Beginning with an unpolarized Rb vapor, the polarization buildup is

$$P_{Rb}(t) = \frac{\gamma_{opt}}{\gamma_{opt} + \Gamma_{SD}}\left[1 - e^{-(\gamma_{opt} + \Gamma_{SD})t}\right],$$

where Γ_{SD} is the bulk Rb spin destruction rate, which depends on Rb collisions with atoms, walls, etc.

The final process is the transfer of polarization from Rb to ^{3}He. At typical pressures (a few ^{3}He), binary collisions between Rb and ^{3}He atoms are the dominant form of polarization exchange. Spin-dependent collisions, described by a Rb–^{3}He interatomic potential $V_1(\mathbf{R})$, constitute the means of Rb spin transfer and relaxation:

$$V_1(\mathbf{R}) = \gamma(R)\mathbf{K} \cdot \mathbf{S} + A(R)\mathbf{I} \cdot \mathbf{S}$$

where $\mathbf{R}$ is the ineratomic separation, $\mathbf{S}$ is the Rb electron spin, $\mathbf{I}$ is the ^{3}He nuclear spin, γ and A are variable coefficients, and $\mathbf{K}$ is the rotational angular momentum of the Rb–^{3}He atomic pair. This potential is in addition to spin independent interactions, $V_0(\mathbf{R})$, which under standard conditions determine classical collision trajectories. The first term of $V_1(\mathbf{R})$ is the spin-rotation interaction, arising from magnetic fields caused by the motion of changes during

the collision. This effect is generally the dominant

relaxation mechanism for the Rb electron spin (i.e., Γ_{SD}

above). The second term, the isotropic hyperfine interaction,

denotes the transfer of polarization between the Rb electrons

and the ^{3}He nuclei with an associated spin exchange rate, γ_{SE}

that depends on the Rb vapor pressure.

Typically, Rb optical pumping is much faster than the

transfer of Rb polarization to the ^{3}He gas. Thus the build-up

of ^{3}He spin polarization can be written as:

$$P_{^3He}(t) = P_{Rb} \frac{\gamma_{SE}}{\gamma_{SE} + \Gamma} \left[1 - e^{-(\gamma_{SE} + \Gamma)t} \right],$$

ignoring the asymptotic Rb polarization, $P_{Rb} \dfrac{\gamma_{SE}}{\gamma_{SE} + \Gamma}$. Here Γ is

the rate of ^{3}He spin depolarization, generally given by ^{3}He-

wall interactions in the glass polarization cell. For typical

parameters, the time to reach equilibrium ^{3}He polarization

(~10 - 30%) is about 10 - 20 hours.

Experimental Setup and Results

We developed a system to produce the ~1 liter quantities

of hyper-polarized ^{3}He needed for human lung imaging. A

photograph of this system is given in Figure 15. The major

components of the noble gas polarization system were: the

polarization chamber, including the cell; the optical pumping

laser; and the magnetic field. A schematic diagram of a

noble gas polarization system is given in Figure 16.

Figure 15. Photograph of polarization cart at Massachusetts General Hospital.
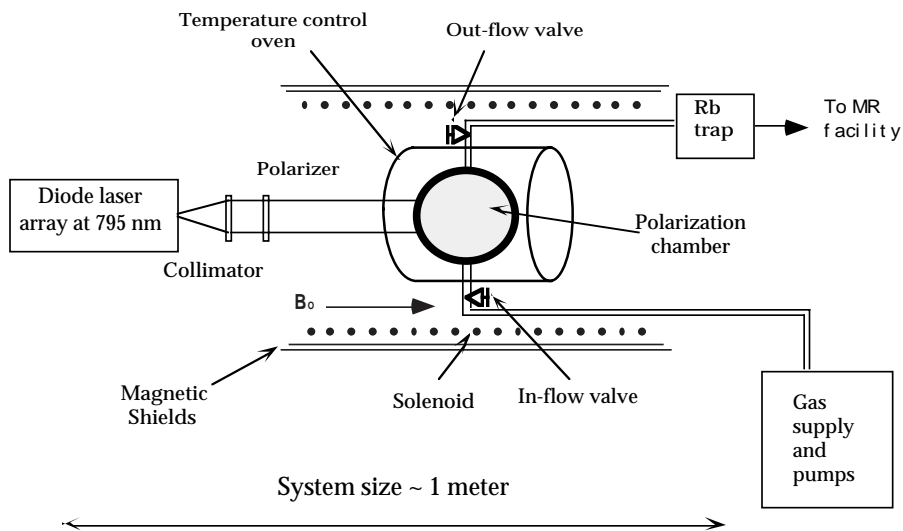
Figure 16. Schematic diagram of a noble gas polarization system.

Two factors that contribute to ^{3}He spin polarization destruction are magnetic field gradients and wall collisions. For this reason the polarization cell was made of Corning 1720 aluminosilicate, which lacks some of the paramagnetic impurities and is less porous than Pyrex. A one inch diameter Pyrex bulb filled with 3 atm of ^{3}He, 1 atm of N_2, and less than a milligram of Rb was used for testing. For the actual lung study a 700 cc valved cell was constructed of aluminosilicate. These cells were acid washed and baked to remove any remaining impurities prior to being filled.

The oven consisted of three concentric cylinders. The inner aluminum cylinder had a glass endcap and a ceramic cap at the opposite end. The aluminum cylinder was encapsulated by two glass cylinders separated by insulation. The cells were heated to 160°C with blown air that entered through a port in the ceramic cap via silicon tubing. The temperature was monitored at the same end by an RTD electronic thermometer. A 3/4 horsepower air compressor maintained an air flow rate of 2.42 cfm, which was heated by an Omega cartridge heater.

A high power (15W) tunable Opto Power laser diode array (LDA) equipped with optical fibers provided the 795 nm light for optical pumping. (This fiber coupled LDA was of the same type used in the injection locking tests described above.) The unpolarized laser light was circularly polarized by

passing through a polarizing beam splitter and then a pair of quarter wave plates. The circular polarized laser light then entered through the glass capped end of the oven to illuminate the cell.

26" diameter Helmholtz coils were used to produce a constant magnetic field to orient the noble gas dipole moments. At 8 amps the two coils produced a 6 gauss field along their axis. The apparatus was placed on a non-magnetic cart that was operated behind the shielding of the GE 3T whole body MRI unit. The fringe field from the 3T magnetic increased the holding field to 8 gauss.

The entire cell was bathed in laser light and heated to 160 ˚C in the oven. It was then allowed to pump for typically 24 hours. The temperature was then slowly ramped down, over the course of an hour, and the cell was removed.

To measure the ^{3}He polarization in the small test cell we used a Varian 2T NMR system. Since the hyper-polarized signal can be ~10^5 times larger than the typical thermally polarized ^{3}He sample, the detected signal had to be attenuated to avoid overloading the pre-amplifier. Therefore 60 dB of attenuation was placed between the NMR signal detection coil and the receiver. The ^{3}He NMR spectrum was obtained using a pulse and detect sequence, where the flip angle was 10˚. A properly tuned solenoid coil detected the ^{3}He NMR signal with a S/N ratio of 4,300. The remaining magnetization was pulsed away,

and the cell was left in the bore of the magnet overnight to allow the ^{3}He spin polarization to establish thermal equilibrium based on the Boltzmann distribution. With the same flip angle as before the thermal sample had a S/N ratio of 4.5. Using the Boltzmann factor we find that the probability of finding ^{3}He in the spin up state at room temperature in a 2T field is

$$P_+ \cong \tanh\left(\frac{\hbar\omega_o}{2kT}\right) = 5.14 \times 10^{-6}.$$

Multiplying by the S/N ratio between the hyper-polarized and thermally polarized sample, we found that the hyper-polarized ^{3}He gas samples had typical polarization of about 2%, less than the target of 10 - 30%, but sufficient for initial studies of human lung ^{3}He MRI at 3 T. Optimization of the ^{3}He polarization system and tests with valved cells are currently underway.

[1] C.E. Hayes, et. al., J. Magn.RReson. **63**, 622 (1985)
[2] J.T. Vaughan Jr., PhD. Dissertation, Univ. of Alabama (1993).
[3] J. Jin, "Electromagnetic Analysis and Design in Magnetic Resonance Imaging", (CRC Press, 1999) p. 194.
[4] A. Kastler, J. Phys. Radium **11**, 255 (1950).